

RESEARCH ARTICLE

Highly resolved modeling of extreme wind speed in North America and Europe

Christopher Jung¹  | Laura Demant²  | Peter Meyer² | Dirk Schindler¹ 

¹Environmental Meteorology,
Albert-Ludwigs-Universität Freiburg,
Freiburg, Germany

²Department of Forest Conservation,
Northwest German Forest Research
Institute, Hann. Münden, Germany

Correspondence

Christopher Jung, Environmental
Meteorology, Albert-Ludwigs-Universität
Freiburg, Werthmannstrasse 10, D-79085
Freiburg, Germany.
Email: christopher.jung@mail.unr.uni-freiburg.de

Funding information

Bundesministerium für Umwelt,
Naturschutz und nukleare Sicherheit,
Grant/Award Number: MiStriKli 28W-K-
4-166-01

Abstract

High wind speed (U) is one of the most dangerous natural hazards in North America and Europe. As a result, spatially explicit, statistical estimation of extreme U is of particular relevance for many sectors. However, the most common sources of wind speed data such as reanalysis data and in situ measurements are limited for this purpose due to their coarse spatial resolution and low representativeness. Thus, the main goal was to develop a high spatial resolution ($250\text{ m} \times 250\text{ m}$) model (GloWiSMo-X) for monthly mapping of the maximum hourly U for a 10-year return period ($U_{10\text{yr}}$) in North America and Europe. The multistep development of GloWiSMo-X is based on 2544 hourly U time series available from the integrated surface global hourly meteorological data set (U_{NCEI}), U time series from ERA5 (U_{ERA5}), and mean wind speed from the Global Wind Speed Model ($\bar{U}_{\text{GloWiSMo}}$). Firstly, the block maxima method was applied to estimate monthly wind speed for a 10-year return period for both U_{NCEI} ($U_{10\text{yr},\text{NCEI}}$) and U_{ERA5} ($U_{10\text{yr},\text{ERA5}}$). Secondly, the least squares boosting approach was used to predict the target variable $U_{10\text{yr},\text{NCEI}}$ yielding the predictions $\hat{U}_{10\text{yr}}$. The predictor variables $U_{10\text{yr},\text{ERA5}}$, $\bar{U}_{\text{GloWiSMo}}$, continent, and month were used as input. It was found that the highest monthly continental means of $\hat{U}_{10\text{yr}}$ ($\bar{U}_{10\text{yr}}$) in January are 16.4 m/s in North America and 16.3 m/s in Europe. $\bar{U}_{10\text{yr}}$ dropped to 13.4 m/s and 12.5 m/s in August. The annual cycle of $\bar{U}_{10\text{yr}}$ is more pronounced in Europe than in North America. The central parts of the USA and Western Europe were identified as intracontinental regions with the highest $\bar{U}_{10\text{yr}}$. GloWiSMo-X proves to be very broadly applicable as it covers two different continents and all months. The model validation by the mean squared error (MSE) demonstrates its improved predictive power compared to ERA5.

KEYWORDS

ERA5, GloWiSMo, LS-Boost, statistical downscaling, wind speed distribution

This is an open access article under the terms of the [Creative Commons Attribution](https://creativecommons.org/licenses/by/4.0/) License, which permits use, distribution and reproduction in any medium, provided the original work is properly cited.

© 2022 The Authors. *Atmospheric Science Letters* published by John Wiley & Sons Ltd on behalf of Royal Meteorological Society.

1 | INTRODUCTION

Catastrophic storms are one of the most damaging natural hazards. In Europe, synoptic-scale storms frequently occur in winter (Feser et al., 2015), while in summer, they are mostly limited to local or regional convective events (Groenemeijer et al., 2017). Among the costliest European storms in recent decades were the winter storms Lothar (year: 1999, total damage: 11,200 US\$m), Kyrill (2007, 8700 US\$m), and Daria (1990, 7000 US\$m) (Munich RE, 2019). Hurricanes (Murakami et al., 2016) and tornadoes (Taszarek, Allen, et al., 2020) are much more relevant in North America than in Europe. For instance, the most damaging hurricane, Katrina, caused 125,000 US\$m total damage (Munich RE, 2019).

Regardless of continent, season, and storm type, one important damage-triggering feature during storms are the associated high wind speed (U) values. As a consequence of their potential for damage formation, spatially explicit knowledge of extreme U is of particular relevance for many sectors, including forestry (Forzieri et al., 2020), insurance (Schwierz et al., 2010), construction (Hay et al., 2019), wind energy (Jung et al., 2017), waterways transport (Valverde & Convertino, 2019), nature conservation (Maxwell et al., 2019), and air traffic (Taszarek, Kendzierski, & Pilgaj, 2020).

Estimating extreme U is complex because each storm's track is unique. Identifying recurring storm field patterns may assist in the statistical assessment of extreme wind speed occurrence probabilities. Related to this, long-term, representative U measurements fitted to theoretical distributions are frequently used for estimating statistical U return values for periods ≥ 10 years.

For instance, the Gumbel distribution was used to estimate extreme U at 42 Brazilian sites (Pes et al., 2017). Various theoretical distributions were applied to assess their capability to mimic North American, extreme U distributions (Morgan et al., 2011). At five globally distributed sites, the inverse Burr distribution was applied for predicting extreme U values (Chiodo & De Falco, 2016). In another study, the five-parameter Wakeby (Wak) distribution and three-parameter generalized extreme value (GEV) distributions were identified as theoretical distributions providing high-fitting accuracy. In that study, return values for 30, 50, and 100 years were estimated on a $1.00^\circ \times 1.00^\circ$ horizontal resolution global grid using ERA-interim reanalysis data (Jung et al., 2017). In a recent study, global estimates of extreme wind speed at a horizontal resolution of $0.25^\circ \times 0.25^\circ$ were developed from ERA5 reanalysis data (Pryor & Barthelmie, 2021).

Typically, storm-related damage varies on more minor spatial scales than those of reanalysis data (Koks & Haer, 2020). Thus, modeling extreme U at finer

grids is required. A combination of a statistical and dynamical downscaling approach was developed to derive extreme U for Europe between 1989 and 2010 (Haas & Pinto, 2012). Extreme U was also simulated in Switzerland on a $50 \text{ m} \times 50 \text{ m}$ horizontal resolution grid (Etienne et al., 2010).

Previous studies reveal that the most common U sources such as reanalysis data and in situ measurements are of limited use for high spatial resolution mapping of extreme U since they are either coarsely resolved or not representative. The existing high spatial resolution models refer to regional scales or are only available for average U conditions. Consequently, the validity for consistent inter- and intracontinental comparison of the spatiotemporal $U_{10\text{yr}}$ pattern is limited. Thus, the goals of this study are (1) to develop a new high spatial resolution ($250 \text{ m} \times 250 \text{ m}$) model (GloWiSMo-X) for monthly mapping of maximum hourly U for a 10-year return period ($U_{10\text{yr}}$) in North America and Europe, (2) to compare the spatiotemporal $U_{10\text{yr}}$ patterns in North America and Europe, and (3) to quantify the improvement of the predictive power of GloWiSMo-X compared to assessments based on reanalysis data.

2 | MATERIAL AND METHODS

2.1 | Wind speed data

The development of GloWiSMo-X is based on three different U data sets available at 10 m above ground level. All data sets cover U data in the period from at least January 01, 1989 to December 31, 2018 in North America and Europe. A consecutive period of 30 years is defined as climate normal by the World Meteorological Organization (2021) and is considered long enough to describe the climate variability (Azorin-Molina et al., 2014).

The first U data set consists of measured hourly U time series from the integrated surface global hourly meteorological data set (U_{NCEI}) archived at NOAA's National Centers for Environmental Information (NCEI, 2019). All time series were subdivided monthly. An essential prerequisite was the completeness of the U_{NCEI} time series. Only monthly U_{NCEI} time series with data availability of at least 90% were considered further. As a result, 9854 sites were sorted out. Monthly U_{NCEI} time series of a total of 2544 sites were further used. An extension of NCEI in situ measurements before 1989 was avoided to not further reduce the number of measurement sites. Of all monthly time series, 37.2% are located in Europe and 62.8% in North America.

The second U data set was available from the ERA5 reanalysis project (Hersbach et al., 2020). It consists of

gridded U (U_{ERA5}) calculated from hourly horizontal wind vector components. The horizontal resolution of ERA5 is $0.25^\circ \times 0.25^\circ$. Analogous to U_{NCEI} , U_{ERA5} was subdivided into monthly time series.

The third U data set was obtained from the Global Wind Speed Model (GloWiSMo) which consists of gridded wind speed distribution parameters for the period January 01, 1989 to December 31, 2018 at $250 \text{ m} \times 250 \text{ m}$ horizontal resolution. GloWiSMo considers the local influences of elevation, relative elevation, curvature, slope, and roughness length on the wind speed distribution (Jung & Schindler, 2020). For this study, GloWiSMo mean wind speed ($\bar{U}_{\text{GloWiSMo}}$) was used. In contrast to the U_{ERA5} time series, the statistical distributions of hourly U comprised in GloWiSMo are only suitable for average U conditions but not for estimating extreme 10-year return periods.

2.2 | Extreme value analysis

The extreme value analysis was made for each of the monthly U_{NCEI} and U_{ERA5} time series. The block maxima method was used for this purpose. It is an efficient method in extreme value theory for estimating return values. The block maxima method is suitable for this investigation since wind speed measurements are not independent and reveal a seasonal pattern (Ferreira & De Haan, 2015). The first step was to extract the monthly annual maxima of U_{NCEI} ($U_{\text{max,NCEI}}$) and U_{ERA5} ($U_{\text{max,ERA5}}$).

GEV (Hosking, 1985) and Wak (Houghton, 1978) distributions were fitted to monthly $U_{\text{max,NCEI}}$ and $U_{\text{max,ERA5}}$. Previous studies revealed that both distributions are capable of reproducing U regimes (Jung & Schindler, 2019b) and are suitable for extreme value analysis (Jung et al., 2017).

The cumulative distribution function (cdf) of GEV is defined as (Houghton, 1978):

$$F_{\text{GEV}}(U_{\text{max}}; \mu, \eta, \iota) = \exp \left\{ - \left[1 + \iota \frac{(U_{\text{max}} - \mu)}{\eta} \right]^{-\frac{1}{\iota}} \right\} \quad (1)$$

where μ is the location, η is the scale, and ι is the shape parameter.

Wak is usually defined by its quantile function (F_{Wak}^{-1}):

$$F_{\text{Wak}}^{-1}(U_{\text{max}}; \alpha, \beta, \gamma, \delta, \varepsilon) = \varepsilon + \frac{\alpha}{\beta} \left[1 - (1 - F)^\beta \right] - \frac{\gamma}{\delta} \left[1 - (1 - F)^{-\delta} \right] \quad (2)$$

with α and γ being the scale, β and δ the shape, and ε being the location parameters. The cdf of Wak was calculated by numerically inverting the quantile function (Rahman et al., 2015).

For GEV parameter estimation the maximum likelihood (Hosking, 1985) and for Wak parameter estimation the L-moment method (Houghton, 1978) were applied.

A 10-year return period corresponds to the 90th percentile of cdf. To obtain robust results, the mean of Wak and GEV was used to calculate $U_{10\text{yr,NCEI}}$ and $U_{10\text{yr,ERA5}}$.

2.3 | LS-Boost modeling

A least squares boosting (LS-Boost) modeling approach (Friedman, 2001) was used for high spatial resolution mapping of extreme wind speed. The target variable for LS-Boost modeling was $U_{10\text{yr,NCEI}}$. To account for the large-scale pattern of extreme wind speed conditions, monthly $U_{10\text{yr,ERA5}}$ was chosen as first predictor variable (PV). $\bar{U}_{\text{GloWiSMo}}$ was applied as second PV to consider the small-scale wind speed properties. Continent (binary) and month (1, ..., 12) were additional PVs. Month was chosen as PV to account for the fact that over the course of the year different storm types cause high $U_{10\text{yr}}$.

The spatial pattern of the target variable and the PVs is shown in Figure 1 exemplarily for Europe. Calculated extreme wind speed in Europe in January based on the target variable $U_{\text{max,NCEI}}$ ($U_{10\text{yr,NCEI}}$) and the first PV $U_{\text{max,ERA5}}$ ($U_{10\text{yr,ERA5}}$) is presented in Figure 1a,b. The second PV $\bar{U}_{\text{GloWiSMo}}$ is displayed in Figure 1c.

The LS-Boost approach was used for modeling $U_{10\text{yr,NCEI}}$ yielding the predictions of $U_{10\text{yr,NCEI}}$ ($\hat{U}_{10\text{yr}}$). According to previous studies, the LS-Boost algorithm is well suitable for small-scale modeling of extreme U (Jung & Schindler, 2019a; Schindler et al., 2016). The LS-Boost approach is based on a sequence of binary regression trees (B_m) that minimize the mean squared error (MSE) between $U_{10\text{yr,NCEI}}$ and $\hat{U}_{10\text{yr}}$. The algorithm begins with the first guess of $U_{10\text{yr,NCEI}}$ by using its median ($\tilde{U}_{10\text{yr,NCEI}}$). Next, multiple regression trees B_1, \dots, B_M are combined in a weighted manner. The LS-Boost regression trees are a function of the PVs $U_{10\text{yr,ERA5}}$, $\bar{U}_{\text{GloWiSMo}}$, continent, and month, (Friedman, 2001; van Heijst et al., 2008):

$$\hat{U}_{10\text{yr}}(\text{PV}) = \tilde{U}_{10\text{yr,NCEI}}(\text{PV}) + lr \sum_{m=1}^M p_m B_m(\text{PV}) \quad (3)$$

with the hyperparameters p_m being the weight for model m , M is the total number of regression trees, and lr equals the learning rate. The LS-Boost method is available in

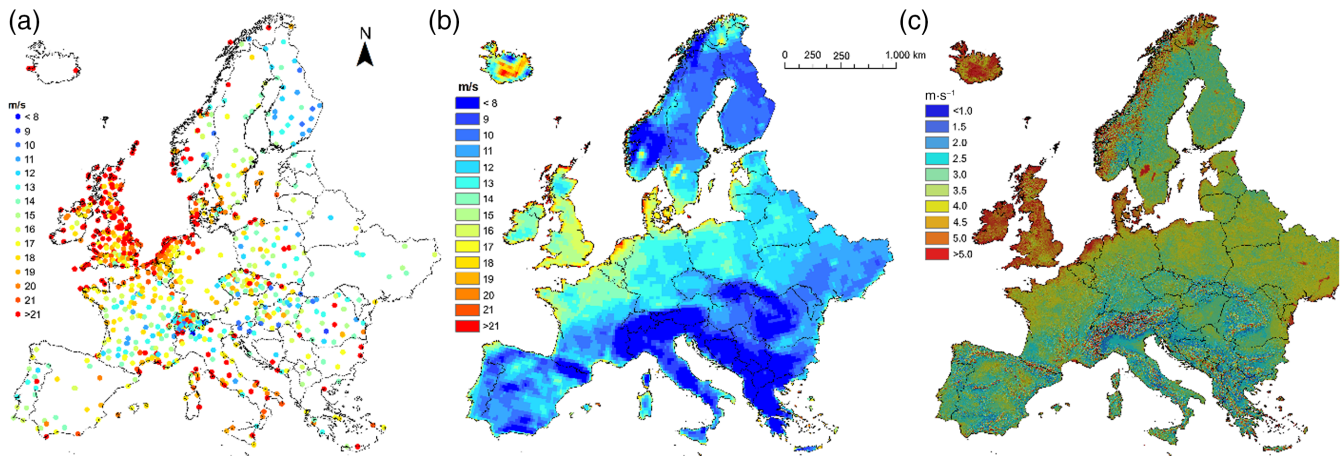


FIGURE 1 Spatial distribution of wind speed for a 10-year return period in January in Europe estimated based on (a) the target variable $U_{10\text{yr},\text{NCEI}}$ from National Centers for Environmental Information data and (b) the first predictor variable $U_{10\text{yr},\text{ERA5}}$ available from ERA5 data. The second predictor variable is the (c) mean wind speed from the global wind speed model ($\bar{U}_{\text{GloWiSMo}}$)

Mathworks' Matlab[®] Software Statistics and Machine Learning Toolbox (Release 2020a; The Math Works Inc.).

The algorithm was applied to a $250 \text{ m} \times 250 \text{ m}$ grid that matches the GloWiSMo grid. This was done by running the LS-Boost regression trees at all grid cells and using the closest ERA5 grid cell as input for $U_{10\text{yr},\text{ERA5}}$. To find the optimal hyperparameterization, combinations of different M and lr values were tested by the MSE which is calculated by the errors (ER) between $\hat{U}_{10\text{yr}}$ and $U_{10\text{yr},\text{NCEI}}$. The finally selected model was then evaluated by fivefold cross-validation yielding the four error measures MSE, mean error (ME), mean absolute error (MAE), and mean absolute percentage error (MAPE) (Willmott, 1982).

Areal means of $\hat{U}_{10\text{yr}}$ ($\bar{U}_{10\text{yr}}$) were computed for both continents and subcontinental regions by averaging all grid cells that belong to a continent or a region using Esri's ArcGIS[®] 10.6 software.

3 | RESULTS AND DISCUSSION

3.1 | Modeled extreme wind speed

The pattern of $\hat{U}_{10\text{yr}}$ is highly variable both in space and in time. To highlight the spatiotemporal $\hat{U}_{10\text{yr}}$ variability, continental $\hat{U}_{10\text{yr}}$ from GloWiSMo-X which was modeled based on the PVs $U_{10\text{yr},\text{ERA5}}$, $\bar{U}_{\text{GloWiSMo}}$, continent, and month is presented for January and July in Figure 2. These months were exemplarily chosen to compare $\hat{U}_{10\text{yr}}$ in winter and summer.

In January, the area where $\hat{U}_{10\text{yr}} > 20 \text{ m} \cdot \text{s}^{-1}$ is 16.1% in North America and 8.2% in Europe. In North America, these areas include the central parts of the United States

and Northern Canada. In Europe, they include Iceland, the British Isles, Denmark, and the Netherlands. Elsewhere, exposed mountain ranges and inland water bodies are exposed to $\hat{U}_{10\text{yr}} > 20 \text{ m} \cdot \text{s}^{-1}$ in both continents. Regions with $\hat{U}_{10\text{yr}} < 12 \text{ m} \cdot \text{s}^{-1}$ are rare. In both Europe and North America, they account for less than 2.0% of the total area. Their occurrence is mostly limited to sheltered valley sites. However, there is a relevant number of regions where $12.0 \text{ m} \cdot \text{s}^{-1} \leq \hat{U}_{10\text{yr}} < 15.0 \text{ m} \cdot \text{s}^{-1}$ (share of area: 44.1% in North America and 37.6% in Europe), indicating a strongly leptokurtic $\hat{U}_{10\text{yr}}$ distribution. These regions comprise southeastern USA, central Alaska, and southwestern Canada. In Europe, they occur in the south in a patchy manner.

In July, $\hat{U}_{10\text{yr}}$ is considerably lower than in January. Since the share of the area is below 1.6%, in both continents, areas where $\hat{U}_{10\text{yr}} > 20 \text{ m/s}$ are hardly identifiable. However, the decline of $\hat{U}_{10\text{yr}}$ from January to July is much more pronounced in Europe than in North America. Especially in the central parts of the United States, $\hat{U}_{10\text{yr}}$ frequently exceeds 15 m/s. During July, the area where $\hat{U}_{10\text{yr}} < 15 \text{ m/s}$ greatly increases to 93.7% in Europe and is 73.6% in North America. In Europe, the regions with $\hat{U}_{10\text{yr}} < 12.0 \text{ m/s}$ account for 40.7% and 26.4% in North America.

The generally higher $\hat{U}_{10\text{yr}}$ values in January can be attributed to the dominance of synoptic-scale storm events in winter in both North America and Europe. During the summer months, synoptic-scale storm events are much less frequent. However, in the summer months, there are more convective storm events which are usually much smaller in spatiotemporal extent than synoptic-scale storm events. This leads to more localized damage in summer than in the winter months.

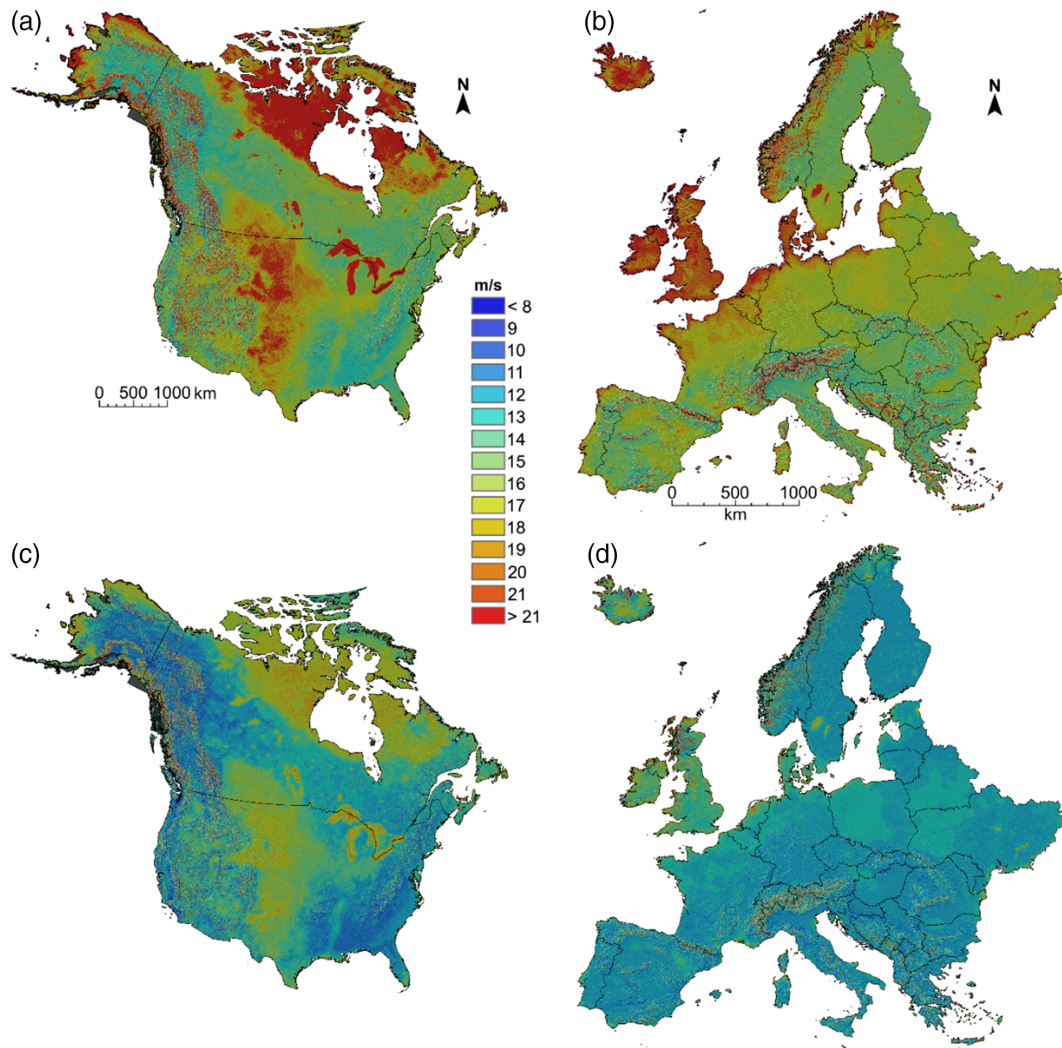


FIGURE 2 Modeled maximum hourly wind speed for a 10-year return period ($\hat{U}_{10\text{yr}}$) in January in (a) North America and (b) Europe and in July in (c) North America and (d) Europe

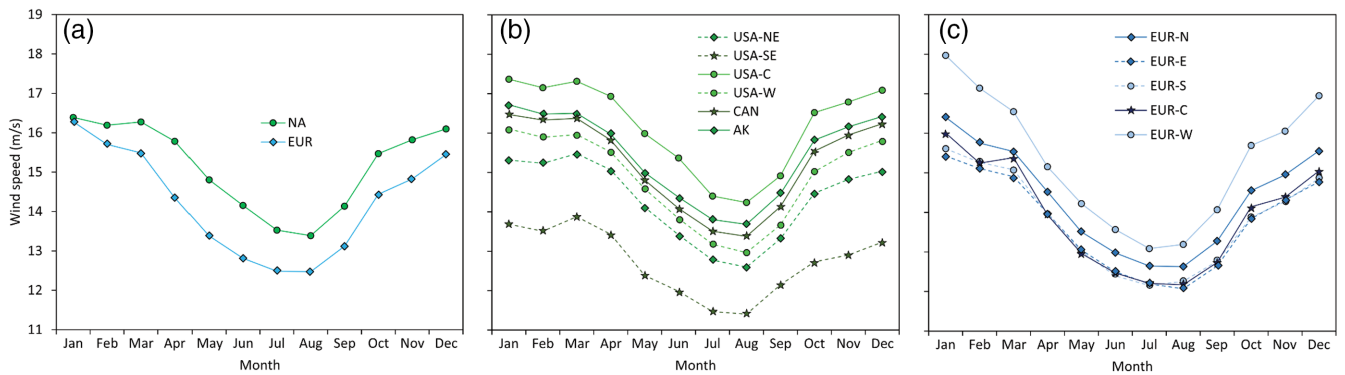


FIGURE 3 Monthly time series of modeled maximum hourly wind speed for a 10-year return period averaged ($\bar{U}_{10\text{yr}}$) across the grids cells ($\bar{U}_{10\text{yr}}$) representing (a) North America (NA) and Europe (EUR); (b) Northeastern USA (USA-NE), Southeastern USA (USA-SE), central parts of the United States (USA-C), Western USA (USA-W), Canada (CAN), and Alaska (AK); and (c) Northern Europe (EUR-N), Eastern Europe (EUR-E), Southern Europe (EUR-S), Central Europe (EUR-C), and Western Europe (EUR-W)

Despite the changed $\hat{U}_{10\text{yr}}$ magnitudes between January and July, the intracontinental geographical patterns of monthly $\hat{U}_{10\text{yr}}$ values are similar.

Monthly time series underline the distinct intra-annual $\bar{U}_{10\text{yr}}$ variability (Figure 3). In North America and Europe, maximum continental $\bar{U}_{10\text{yr}}$ occurs in January. The $\bar{U}_{10\text{yr}}$ minima were modeled for August. In January, continental $\bar{U}_{10\text{yr}}$ is 16.4 m/s in North America and 16.3 m/s in Europe. In August, $\bar{U}_{10\text{yr}}$ decreases to 13.4 m/s in North America and 12.5 m/s in Europe, respectively. The continental $\bar{U}_{10\text{yr}}$ differences, North America minus Europe, are greater from April to November (1.2 m/s) compared to the period December to March (0.5 m/s). Furthermore, $\bar{U}_{10\text{yr}}$ reveals major intracontinental variations. The central parts of the United States and Western Europe have the highest $\bar{U}_{10\text{yr}}$ values.

In January, $\bar{U}_{10\text{yr}}$ in western Europe (18.0 m/s) exceeds $\bar{U}_{10\text{yr}}$ in the central parts of the United States (17.4 m/s). The region with the lowest $\bar{U}_{10\text{yr}}$ level

comprises southeastern parts of the United States where $\bar{U}_{10\text{yr}} < 14.0$ m/s. In Eastern, Southern, and Central Europe, $\bar{U}_{10\text{yr}}$ is almost identical from June to September at a very low level ($\bar{U}_{10\text{yr}} < 13.0$ m/s).

Map extracts of $\hat{U}_{10\text{yr}}$ centered around New York State and Switzerland are presented in Figure 4 to highlight the small-scale $\hat{U}_{10\text{yr}}$ variations. These regions were selected because they both encompass very complex terrain yielding a great $\hat{U}_{10\text{yr}}$ contrast.

Regardless of the modeled month, $\hat{U}_{10\text{yr}}$ values are very high in the exposed mountain ranges in both map extracts. In New York State, noticeably high $\hat{U}_{10\text{yr}}$ values occur in the Catskill Mountains which are a part of the Appalachian Mountains. In Switzerland, the exposed summits of the Alps are strongly affected by high $\hat{U}_{10\text{yr}}$ values. In addition to the topographic influences on $\hat{U}_{10\text{yr}}$, the roughness influence on $\hat{U}_{10\text{yr}}$ is also emphasized by the map extracts. With increasing proximity to the US Atlantic coast, the $\hat{U}_{10\text{yr}}$ values

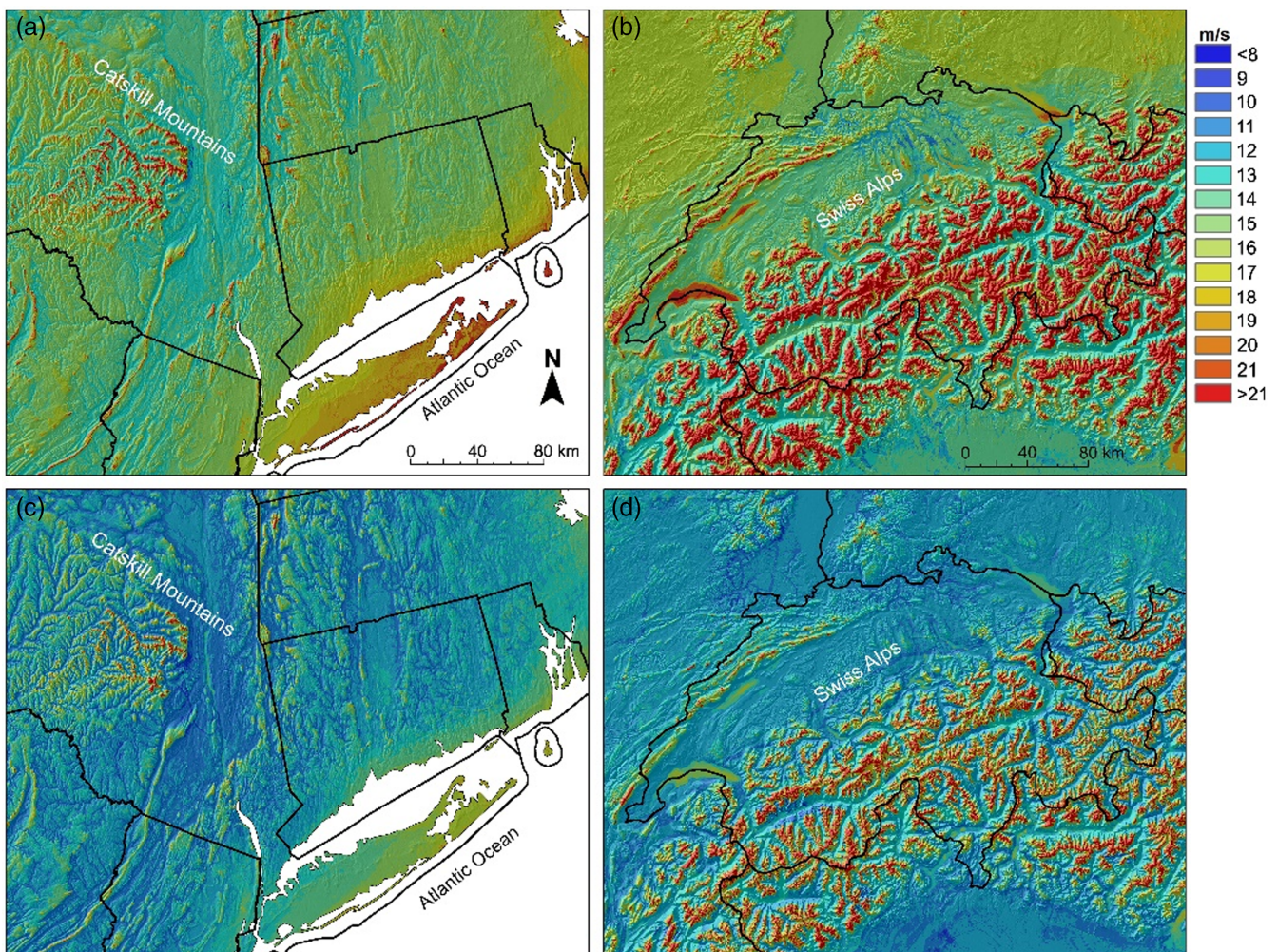


FIGURE 4 Modeled maximum hourly wind speed for a 10-year return period ($\hat{U}_{10\text{yr}}$) in January centered around (a) New York state and (b) Switzerland and in July centered around (c) New York state and (d) Switzerland

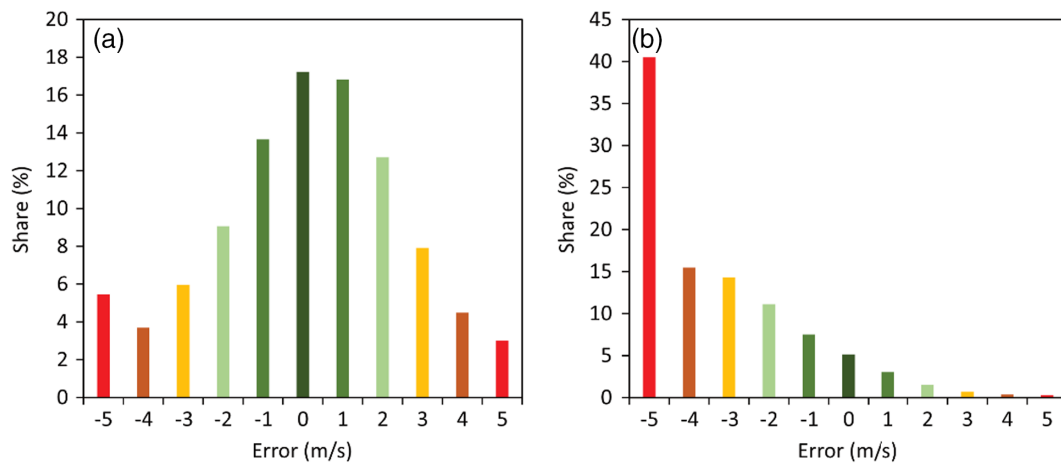


FIGURE 5 Error histogram (ER) for (a) GloWiSMo-X ($ER = \hat{U}_{10yr} - U_{10yr,NCEI}$) and (b) ERA5 ($ER = U_{10yr,ERA5} - U_{10yr,NCEI}$)

increase considerably. Furthermore, inland water bodies lead to higher \hat{U}_{10yr} values compared with the surrounding area.

3.2 | Model validation

The error histograms for GloWiSMo-X ($ER = \hat{U}_{10yr} - U_{10yr,NCEI}$) and ERA5 ($ER = U_{10yr,ERA5} - U_{10yr,NCEI}$) are displayed in Figure 5 to quantify the improvement of the predictive power of GloWiSMo-X for extreme wind speed simulation compared to ERA5. The model validation for ERA5 reveals a distinct bias between $U_{10yr,ERA5}$ and $U_{10yr,NCEI}$ with $ME = -4.2$ m/s. This bias was fully corrected by GloWiSMo-X ($MSE = 0.0$ m/s). The greater bias of ERA5 may be due to the fact that rare storm events are simulated worse by ERA5 than average conditions. In particular, convective events are more poorly simulated due to their short spatiotemporal extent. In contrast, GloWiSMo-X uses actual measurements as target variables which reflect the general level of extreme wind speed. The further error measures also indicate considerable improvements of the predictive power of GloWiSMo-X ($MSE = 7.2$ m/s, $MAE = 2.0$ m/s, and $MAPE = 14.3\%$) compared to ERA5 ($MSE = 31.9$ m/s, $MAE = 4.5$ m/s, and $MAPE = 28.6\%$).

For GloWiSMo-X, 17.2% of all evaluated predictions, \hat{U}_{10yr} and $U_{10yr,NCEI}$ agree. For another 30.5% of all predictions, $ER = |1 \text{ m} \cdot \text{s}^{-1}|$. Overall, the errors for 69.5% of all predictions are in the range of -2 to $+2$ m/s indicating a sufficient model accuracy. However, for 16.6% of all predictions, $ER \geq |4 \text{ m} \cdot \text{s}^{-1}|$.

The GloWiSMo-X parameterization using $M = 90$ and $lr = 0.20$ provided the lowest MSE. Thus, this combination was selected for the final \hat{U}_{10yr} model.

4 | CONCLUSIONS

In this study, monthly extreme wind speed for a 10-year return period was mapped on a high spatial resolution scale ($250 \text{ m} \times 250 \text{ m}$) by the newly developed model GloWiSMo-X in North America and Europe. The main similarities between North America and Europe include a distinctive annual U_{10yr} pattern with the maximum in January and the minimum in August and similar effects of exposure and roughness on U_{10yr} . In contrast, the main differences are a greater magnitude of the annual cycle, and usually smaller variations of U_{10yr} between intracontinental regions in Europe than North America.

The developed model proves to be very broadly applicable as it covers two different continents and all months. The model validation also indicates that GloWiSMo-X outperforms the accuracy of the coarser resolved ERA5 reanalysis data set. Besides, the probabilistic nature of GloWiSMo-X allows overcoming the limited informative value of the evaluation of specific individual storm events. It enables spatially explicit statements about storm hazard statistics. These attributes make GloWiSMo-X beneficial for numerous sectors and applications, including forestry, insurance, local planning, the wind industry, nature conservation, and air traffic. In addition, GloWiSMo-X allows direct comparisons of both continents (e.g., comparison of disturbance regimes between North America and Europe). Ultimately, GloWiSMo-X may lead to improved risk management when integrated into storm damage models.

In future studies, GloWiSMo-X may be extended to other continents and more extended return periods. However, the development of highly resolved extreme wind speed fields requires a representative number of long-term wind speed time series. It is anticipated that

the reduced availability of long-term wind speed time series in many other countries complicates the development of such models, and the model accuracy may be worse. Another future goal may be to determine climate change-related changes in the spatiotemporal extreme wind speed pattern and integrate them statistically into GloWiSMo-X.

Further meteorological conditions not integrated in GloWiSMo-X influence storm damage formation. It is relevant whether the high wind speed occurs in conjunction with heavy precipitation, snow, and/or flooding. Also, the type of storm event may lead to different levels of damage. The gustiness of the wind and the duration of the event differ depending on whether it is a synoptic-scale or convective wind event. To incorporate these features, GloWiSMo-X can be parameterized storm type-specific in future studies. This, however, requires an in-depth data preparation in which the wind events are already selected storm type-specific at the beginning. For the consideration of very small-scale convective events which are not fully covered by the NCEI measurement sites, it may also be necessary to include additional data sources (e.g., radar).

ACKNOWLEDGEMENT

This work was supported by the Federal Ministry for the Environment, Nature Conservation and Nuclear Safety within the framework of the Forest Climate Fund (MiS-triKli 28W-K-4-166-01). We thank the National Centers for Environmental Information and European Centre for Medium-Range Weather Forecasts for providing the NCEI and ERA5 wind speed data.


AUTHOR CONTRIBUTIONS

Christopher Jung: Conceptualization; data curation; formal analysis; investigation; methodology; project administration; resources; software; supervision; validation; visualization; writing – original draft; writing – review and editing. **Laura Demant:** Conceptualization; writing – review and editing. **Peter Meyer:** Conceptualization; writing – review and editing. **Dirk Schindler:** Conceptualization; data curation; formal analysis; investigation; methodology; project administration; resources; software; supervision; validation; visualization; writing – original draft; writing – review and editing.

CONFLICT OF INTEREST

The authors declare that they have no known competing financial interests or personal relationships that could have appeared to influence the work reported in this article.

ORCID

Christopher Jung  <https://orcid.org/0000-0001-5952-2610>

Laura Demant  <https://orcid.org/0000-0002-6108-2340>

Dirk Schindler  <https://orcid.org/0000-0002-9473-6240>

REFERENCES

- Azorin-Molina, C., Vicente-Serrano, S.M., McVicar, T.R., Jerez, S., Sanchez-Lorenzo, A., López-Moreno, J.I. et al. (2014) Homogenization and assessment of observed near-surface wind speed trends over Spain and Portugal, 1961–2011. *Journal of Climate*, 27, 3692–3712.
- Chiodo, E. & De Falco, P. (2016) Inverse Burr distribution for extreme wind speed prediction: genesis, identification and estimation. *Electric Power Systems Research*, 141, 549–561.
- Etienne, C., Lehmann, A., Goyette, S., Lopez-Moreno, J.I. & Beniston, M. (2010) Spatial predictions of extreme wind speeds over Switzerland using generalized additive models. *Journal of Applied Meteorology and Climatology*, 49, 1956–1970.
- Ferreira, A. & De Haan, L. (2015) On the block maxima method in extreme value theory: PWM estimators. *Annals of Statistics*, 43, 276–298.
- Feser, F., Barcikowska, M., Krueger, O., Schenk, F., Weisse, R. & Xia, L. (2015) Storminess over the North Atlantic and north-western Europe – a review. *Quarterly Journal of the Royal Meteorological Society*, 141, 350–382.
- Forzieri, G., Pecchi, M., Girardello, M., Mauri, A., Klaus, M., Nikolov, C. et al. (2020) A spatially explicit database of wind disturbances in European forests over the period 2000–2018. *Earth System Science Data*, 12, 257–276.
- Friedman, J. (2001) Greedy function approximation: a gradient boosting machine. *Annals of Statistics*, 29, 1189–1232.
- Groenemeijer, P., Púčik, T., Holzer, A.M., Antonescu, B., Riemann-Campe, K., Schultz, D.M. et al. (2017) Severe convective storms in Europe: ten years of research and education at the European Severe Storms Laboratory. *Bulletin of the American Meteorological Society*, 98, 2641–2651.
- Haas, R. & Pinto, J.G. (2012) A combined statistical and dynamical approach for downscaling large-scale footprints of European windstorms. *Geophysical Research Letters*, 39, L23804.
- Hay, J.E., Hartley, P. & Roop, J. (2019) Climate risk assessments and management options for redevelopment of the parliamentary complex in Samoa, South Pacific. *Weather and Climate Extremes*, 25, 100214.
- Hersbach, H., Bell, B., Berrisford, P., Hirahara, S., Horányi, A., Muñoz-Sabater, J. et al. (2020) The ERA5 global reanalysis. *Quarterly Journal of the Royal Meteorological Society*, 146, 1999–2049.
- Hosking, J.R. (1985) Algorithm as 215: maximum-likelihood estimation of the parameters of the generalized extreme-value distribution. *Journal of the Royal Statistical Society Series C (Applied Statistics)*, 34, 301–310.
- Houghton, J.C. (1978) Birth of a parent: the Wakeby distribution for modeling flood flows. *Water Resources Research*, 14, 1105–1109.
- Jung, C. & Schindler, D. (2019a) Historical winter storm atlas for Germany (GeWiSA). *Atmosphere*, 10, 387.
- Jung, C. & Schindler, D. (2019b) Wind speed distribution selection—a review of recent development and progress. *Renewable and Sustainable Energy Reviews*, 114, 109290.
- Jung, C. & Schindler, D. (2020) Integration of small-scale surface properties in a new high resolution global wind speed model. *Energy Conversion and Management*, 210, 112733.

- Jung, C., Schindler, D., Buchholz, A. & Laible, J. (2017) Global gust climate evaluation and its influence on wind turbines. *Energies*, 10, 1474.
- Koks, E.E. & Haer, T. (2020) A high-resolution wind damage model for Europe. *Scientific Reports*, 10, 1–11.
- Maxwell, S.L., Butt, N., Maron, M., McAlpine, C.A., Chapman, S., Ullmann, A. et al. (2019) Conservation implications of ecological responses to extreme weather and climate events. *Diversity and Distributions*, 25, 613–625.
- Morgan, E.C., Lackner, M., Vogel, R.M. & Baise, L.G. (2011) Probability distributions for offshore wind speeds. *Energy Conversion and Management*, 52, 15–26.
- Munich RE. (2019) Munich Re's NatCatSERVICE. Available at: <https://natcatservice.munichre.com/> [Accessed 28th May 2019].
- Murakami, H., Vecchi, G.A., Villarini, G., Delworth, T.L., Gudgel, R., Underwood, S. et al. (2016) Seasonal forecasts of major hurricanes and landfalling tropical cyclones using a high-resolution GFDL coupled climate model. *Journal of Climate*, 29, 7977–7989.
- National Centers for Environmental Information. (2019) Integrated Surface Database (ISD). Available at: <https://www.ncdc.noaa.gov/isd/> [Accessed 01st October 2019].
- Pes, M.P., Pereira, E.B., Marengo, J.A., Martins, F.R., Heinemann, D. & Schmidt, M. (2017) Climate trends on the extreme winds in Brazil. *Renewable Energy*, 109, 110–120.
- Pryor, S.C. & Barthelmie, R.J. (2021) A global assessment of extreme wind speeds for wind energy applications. *Nature Energy*, 6, 268–267.
- Rahman, A., Zaman, M.A., Haddad, K., El Adlouni, S. & Zhang, C. (2015) Applicability of Wakeby distribution in flood frequency analysis: a case study for eastern Australia. *Hydrological Processes*, 29, 602–614.
- Schindler, D., Jung, C. & Buchholz, A. (2016) Using highly resolved maximum gust speed as predictor for forest storm damage caused by the high-impact winter storm Lothar in Southwest Germany. *Atmospheric Science Letters*, 17, 462–469.
- Schwierz, C., Köllner-Heck, P., Mutter, E.Z., Bresch, D.N., Vidale, P.L., Wild, M. et al. (2010) Modelling European winter wind storm losses in current and future climate. *Climatic Change*, 101, 485–514.
- Taszarek, M., Allen, J.T., Půček, T., Hoogewind, K.A. & Brooks, H.E. (2020) Severe convective storms across Europe and the United States. Part II: ERA5 environments associated with lightning, large hail, severe wind, and tornadoes. *Journal of Climate*, 33, 10263–10286.
- Taszarek, M., Kendzierski, S. & Pilgus, N. (2020) Hazardous weather affecting European airports: climatological estimates of situations with limited visibility, thunderstorm, low-level wind shear and snowfall from ERA5. *Weather and Climate Extremes*, 28, 100243.
- Valverde, L.J. & Convertino, M. (2019) Insurer resilience in an era of climate change and extreme weather: an econometric analysis. *Climate*, 7, 55.
- van Heijst, D., Potharst, R. & van Wezel, M.A. (2008) Support system for predicting eBay end prices. *Decision Support Systems*, 44, 970–982.
- Willmott, C.J. (1982) Some comments on the evaluation of model performance. *Bulletin of the American Meteorological Society*, 63, 1309–1313.
- World Meteorological Organization. (2021) WMO Climatological Normals. Available at: <https://community.wmo.int/wmo-climatological-normals> [Accessed 21st December 2021].

How to cite this article: Jung, C., Demant, L., Meyer, P., & Schindler, D. (2022). Highly resolved modeling of extreme wind speed in North America and Europe. *Atmospheric Science Letters*, 23(5), e1082. <https://doi.org/10.1002/asl.1082>